Enzyme-Responsive Release of Doxorubicin from Monodisperse Dipeptide-Based Nanocarriers for Highly Efficient Cancer Treatment In Vitro

He Zhang, Jinbo Fei, Xuehai Yan, Anhe Wang, and Junbai Li**

Small aldehyde molecule are demonstrated to induce cationic diphenylalanine to assemble into monodisperse enzyme-responsive nanocarriers with high biocompatibility and excellent biodegradability. The formation of Schiff base covalent bond and accompanying π–π interaction of aromatic rings are found to be the mainly driving forces for the assembly of the nanocarriers. Interestingly, the nanocarriers show autofluorescence due to the n–π^* transitions of C = N bonds, which lends them visually traceable property in living cells. Importantly, the nanocarriers can be taken in by cells and biodegraded in the cells. In addition, doxorubicin is easily loaded into the nanocarriers with high encapsulation amount, and its release can be triggered by tyrisin under physiological conditions. Noticeably, even at a very low drug concentration, the doxorubicin-loaded nanocarriers still exhibit a much higher killing capacity of HeLa cells in vitro, compared to the equivalent-dose free doxorubicin, indicating they have a great potential biomedical application.

1. Introduction

Advanced drug delivery systems have obtained tremendous attention in biomedical applications because of their improved bioavailability, enhanced pharmacokinetics, increased cell uptake and pinpointed intracellular drug release.[1] In nature, many supramolecular assemblies can alter their conformations and chemical structures responding to environmental changes. Inspired by this, stimuli-responsive nanocarriers have been fabricated for many disease treatments.[2] Up to now, endogenous variations of local microenvironment in the disease sites (pH,[3] enzymes,[4] and redox-potential,[5] etc.), exogenous triggers (such as temperature,[6] light,[7] and magnetic field[8] and their combinations[9] have been exploited to realize desirable drug delivery. However, it is still a great challenge to design and develop novel approaches to prepare smart nanocarriers with high biocompatibility and excellent biodegradability for controlled drug release.

Biomolecules such as DNA, lipid, peptides and proteins have been extensively utilized as remarkable building blocks to self-assemble versatile functional nanomaterials for biomedical applications, such as drug delivery, tissue engineering and gene therapy.[10] Among them, diphenylalanine (FF) and its derivates originating from the Alzheimer's β-amyloid polypeptide, as its core recognition motifs for molecular self-assembly,[11] have attracted much interest due to their structural simplicity, ease of chemical modification,[12] biocompatibility[10g,13] and especially strongly capability of assembly under different kinds of conditions.[10e,11,14] In a few pioneering works, FF has been paid great attention on its self-assembly in forming nanotubes and vesicles.[11,13b] In our previous reports, many FF-based microstructures such as organogels,[13c] microcrystals,[14e] and 3D peony-flower-like hierarchical mesocrystals[14f] were prepared by using different solvents.

In this report, we found that the small aldehyde molecule could induce cationic diphenylalanine (CDP) to assemble into nearly monodisperse enzyme-responsive nanoparticles. To our best knowledge, this is the first time to get such stable structure based on FF and they have shown the high biocompatibility and excellent biodegradability. **Scheme 1**a shows the relevant chemical reaction. In detail, the oligomeric glutaraldehyde (2GA and 3GA) could be formed through intermolecular aldol reaction.[15] Then, Schiff base covalent bond was formed through the reaction between aldehyde groups in the oligomers and amino groups in CDP, generating bola-like CDP-2GA-CDP and CDP-3GA-CDP units. The units

H. Zhang, Dr. J. Fei, Prof. J. Li
Beijing National Laboratory for Molecular Sciences
CAS Key Laboratory of Colloid
Interface and Chemical Thermodynamics
Institute of Chemistry
Chinese Academy of Sciences
Beijing 100190, China
E-mail: jbli@iccas.ac.cn
Prof. X. Yan
National Key Laboratory of Biochemical Engineering
Institute of Process Engineering
Chinese Academy of Sciences
Beijing 100190, China
E-mail: yanxh@home.ipe.ac.cn
Dr. A. Wang
National Center for Nanoscience and Technology
Beijing 100190, China

DOI: 10.1002/adfm.201403119

ADVANCED FUNCTIONAL MATERIALS
www.afm-journal.de

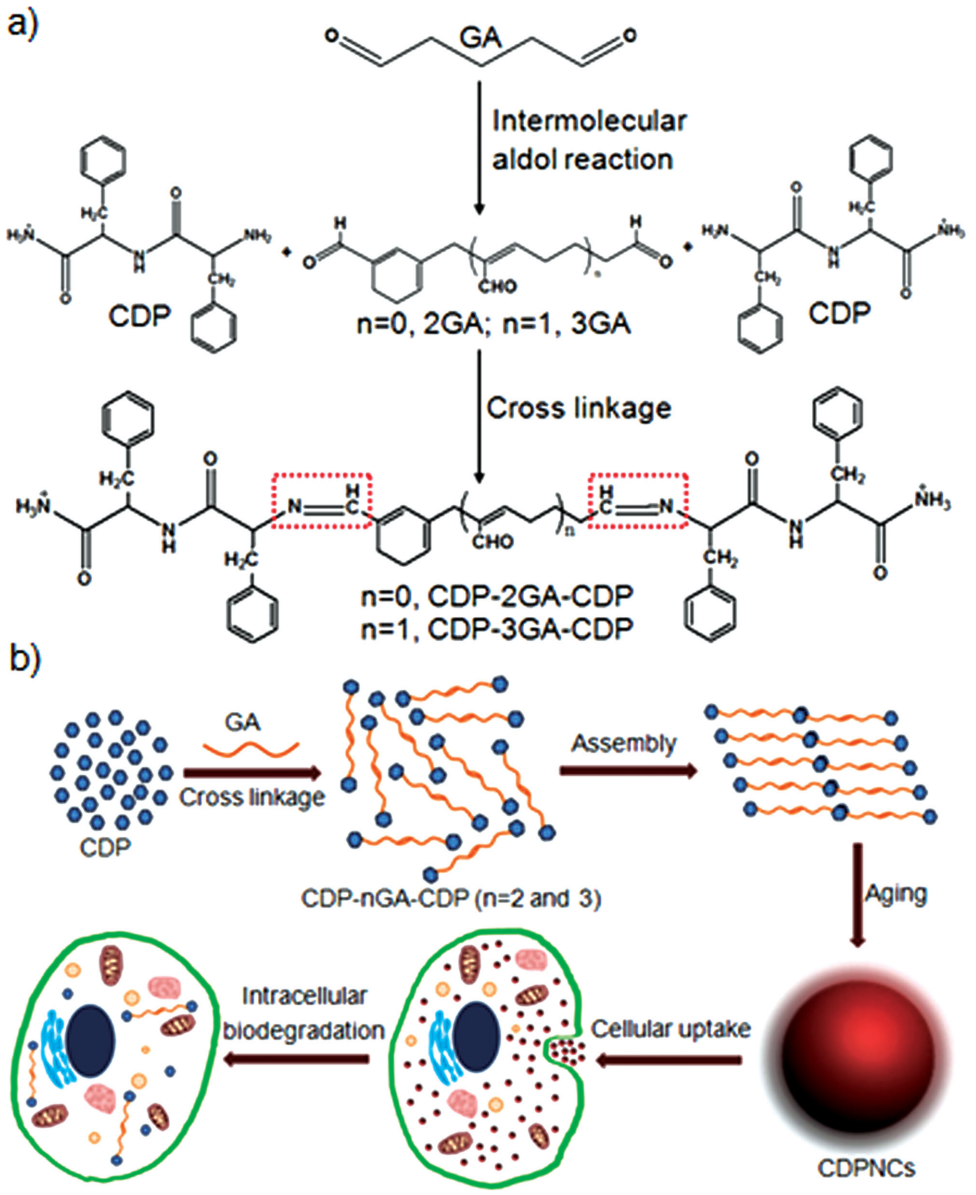

Scheme 1. a) The formation of bola-like CDP-2GA-CDP and CDP-3GA-CDP through Schiff base covalent bond by a cross linkage reaction between CDP and GA. b) A schematic illustration of the assembly of CDPNCs and their intracellular biodegradation.

self-assembled into CDP nanocarriers (CDPNCs) by further aging. The CDPNCs could be taken in by cancer cells and finally degraded in the cells (Scheme 1b). The flexible and facile strategy presented in this work will provide new opportunities to design and develop amino acid-based nanoparticles with versatile biofunctions. Furthermore, the CDPNCs exhibit an adaptive trait of encapsulating various small guest molecules and a desirable enzyme-sensitive nature. Specially, the drug-encapsulation and enzyme-responsiveness of the CDPNCs were evaluated by using doxorubicin (DOX) as a representative anticancer drug. Notably, compared with free DOX, even at a very low drug concentration, the DOX-loaded CDPNCs displayed much higher cytotoxicity in vitro after incubation with tumor cells.

2. Results and Discussion

2.1. Synthesis and Characterization of CDPNCs

In a typical experiment, the CDPNCs were initially prepared by adding an aqueous solution of GA to a 1,1,1,3,3,3-hexafluoro-2-propanol (HFP) solution of CDP with a molar ratio of GA to CDP 1:1. At the beginning, such a mixture was a clear solution. Then, an opalescent and cloudy suspension emerged after aging for 24 h at room temperature (Figure S1, Supporting Information), indicative of the formation of some assembly in the system. After separation and purification, as shown in **Figure 1**, the precipitates were characterized by scanning electron microscopy (SEM), transmission electron microscopy

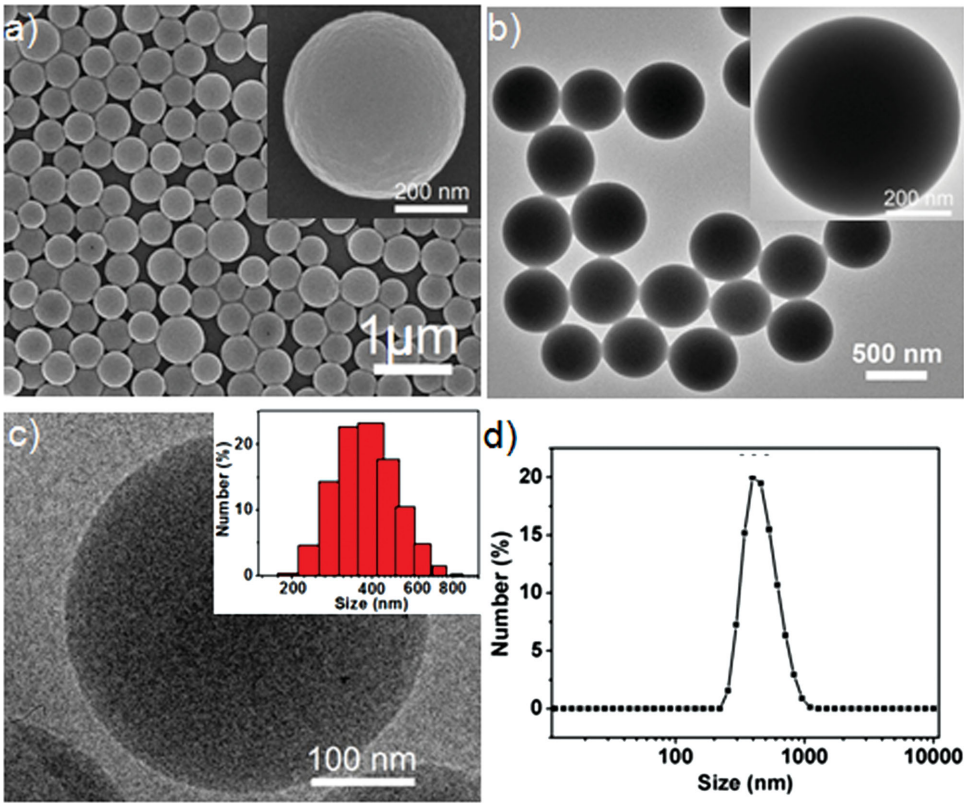

Figure 1. a) SEM images of CDPNCs (Inset: magnified SEM image of a single CDPNC). b) TEM images of CDPNCs (Inset: magnified TEM image of a single CDPNC). c) Cryo-TEM image of a single CDPNC (Inset: A histogram for size-distribution of CDPNCs based on the TEM measurement). d) Size-distribution of CDPNCs measured by DLS (PDI = 0.030).

(TEM) and dynamic light scattering (DLS) measurement. Figure 1a reveals the product is uniform nanospheres with the diameter of about 450 nm. The regular spherical structure is also demonstrated by TEM and homogenous contrast presents the typical characteristic of solid nanospheres (Figure 1b). Further, cryo-TEM image (Figure 1c) of a single nanosphere in situ shows that its contrast decreases gradually from the center to edge, which has a good agreement with the TEM result. Based on the TEM measurement, a histogram is obtained and reveals that the size of nanospheres is about 450 nm (Inset in Figure 1c). The hydrodynamic diameter of CDPNCs in DLS measurement (Figure 1d) is about 480 nm, which is close to the results estimated by SEM and TEM. The surface charge of CDPNCs is positive (+28 mV) because of the existence of the protonated amino groups on the surface of the assembly. Integrating these results above, we can infer that the CDP can react with GA to form CDPNCs in ultra-pure water. It should be noted that if the ultra-pure water was added to the CDP/HFP solution, the above phenomena would not appear and vesicles would be obtained after aging.[13b]

Fourier transform infrared spectroscopy (FTIR) spectra are displayed in **Figure 2**a before and after the introduction of GA. CDP spectrum (red curve) shows typical amino I in the range from 1600 to 1700 cm^{-1}, and the absorption at 1641 cm^{-1} is obviously stronger than the absorption at 1676 cm^{-1}, indicating a predominant parallel β-sheet configuration. In contrast, in CDPNCs spectrum (black curve), the absorption at 1683 cm^{-1} remarkably increases and the absorption at 1605 cm^{-1} almost vanishes, which is indicative of an anti-parallel configuration.[14e,16] Compared with CDP spectrum, it is implied that structural transitions occur in CDPNCs. Although the weak absorption of C = N stretching at 1600 cm^{-1} is masked by typical amino I at 1605 cm^{-1}, the absorption intensity at 1409 cm^{-1} is increased, which is the merging of peak at 1429, 1415, and 1389 cm^{-1} and a characteristic absorption of the C = N.[17] In addition, the intensity at 2934 cm^{-1} in CDPNCs, deriving from the C–H stretching of the Schiff base,[17] also dramatically increases. Hence, the apparent variation of FTIR spectra suggests that CDP can react with GA to form Schiff base bond, which is further confirmed by X-ray photoelectron spectroscopy (XPS) in Figure 2b. A peak at about 401.7 eV emerges in pattern of CDP, which corresponds to the terminal protonated N element of amino groups. However, a new peak at 400.2 eV occurs in pattern of CDPNCs by comparing the N element spectrum of CDP, which is attributed to the formation of C = N. Taken together, Schiff base bond is formed by CDP reacting with GA, resulting in the formation of CDPNCs.

The molecular structure forming CDPNCs was further identified by the matrix-assisted laser desorption/ionization time-of-flight mass spectrometry (MALDI-TOF-MS) in Figure S2 (Supporting Information). The spectrum of CDP includes a characteristic peak at 334 m/z, which is indicative of $CDPNa^+$. As a comparison, the peak of CDP molecule is not observed and a typical new peak emerges at 751 and 832 m/z in the spectrum

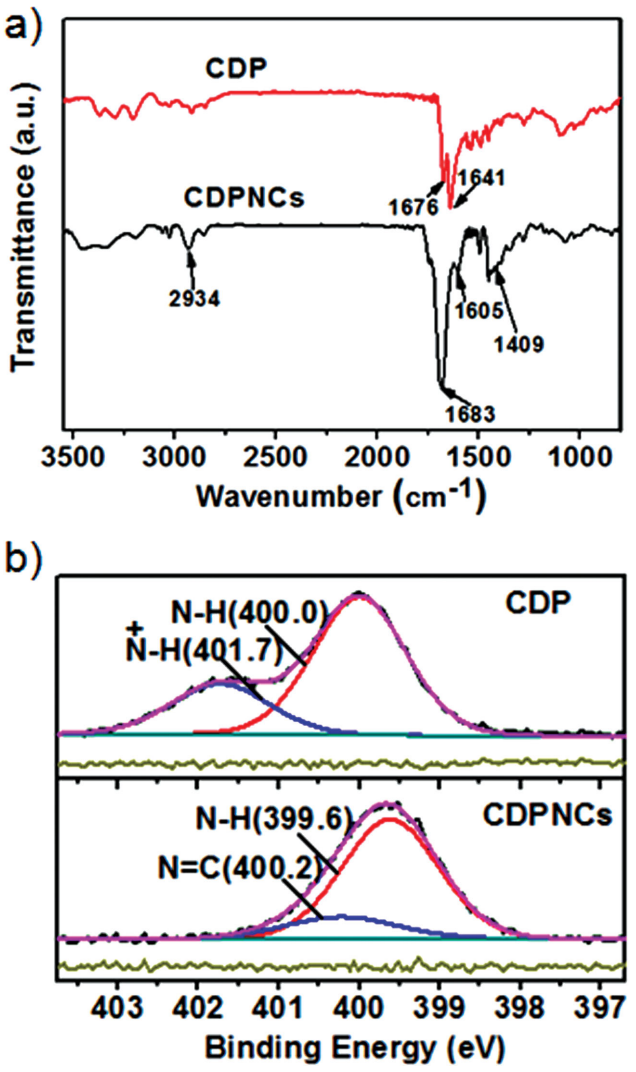

Figure 2. a) FTIR spectra of CDP and CDPNCs powder. b) XPS patterns of N element of CDP and CDPNCs powder.

of CDPNCs, which can be assigned to CDP-2GA-CDPH$^+$ and CDP-3GA-CDPH$^+$, respectively. It can be deduced that the oligomeric GA can be formed through the aldol reaction[15] and then reacts with CDP to form CDP-2GA-CDP and CDP-3GA-CDP (Scheme 1a). Subsequently, thermogravimertric analysis (TGA) curve of the CDPNCs (Figure S3) shows that the weight loss at about 100 °C is ascribed to the release of free water molecules embedded in the CDPNCs, revealing small amount of water molecules might participate in assembly toward the formation of CDPNCs through hydrogen bond.[18] In particular, scarcely any weight loss at 175 °C, indicating that CDP molecules are not included in the CDPNCs. It is in accordance with previous reports[14c,e,18,19] and the MS result above.

In order to further illustrate the formation mechanism of the CDPNCs, time-dependent size and surface potential of CDPNCs assembled were investigated. As shown in Figure S4, the nucleus is quickly formed within 2 min, and then the corresponding nuclei grow slowly in a few hours to form relatively bigger CDPNCs. After aging for 24 h, the size and surface potential of CDPNCs keep almost constant. According to these results, it can be inferred that CDP react with GA through the formation of Schiff base bond to produce CDP-2GA-CDP and CDP-3GA-CDP with poor solubility, which further assembles into smaller nuclei and the corresponding nuclei grow slowly until an arrival of equilibrium. Therefore, the formation mechanism of CDPNCs is involved with nucleation-controlled growth. The strategy to fabricate CDPNCs proposed in this work also can be used to prepared other amino acid-based nanoparticles, such as phenylalanine (F), having the similar chemical structure to CDP. As displayed in Figure S5, the uniform phenylalanine nanospheres were successfully prepared through this method.

Autofluorescent microspheres as novel biological traceable materials have acquired a considerable amount of research interest.[20] The autofluorescent property of CDPNCs was investigated by fluorescence emission spectrum (FL) and confocal laser scanning microscopy (CLSM). The FL spectrum of CDPNCs (Figure S6, Supporting Information) excited by 290 nm displays a broad emission area within the range from 350 to 550 nm due to the formation of Schiff base,[21] which is further confirmed by CLSM images of CDPNCs in water in Petri dishes. When the CDPNCs are excited at 405 nm by laser, multi-wave autofluorescent nature of the CDPNCs in three bands, blue (430–480 nm), green (500–550 nm) and red (590–640 nm), is exhibited in **Figure 3**. The remarkable autofluorescent property of CDPNCs can be attributed to the n-π^* transitions of C = N bonds in the Schiff base.[17a,b,20,22] The autofluorescent nanocarriers, as a potential biological traceable materials, have been proved to gain remarkable advantages over fluorochrome-labled nanocarriers because of avoiding the influence of any external addition.[17a,b,20a,22]

2.2. Stability at Different Dispersion, Cell Uptake, and Enzymatic Biodegradation of CDPNCs

The stability of CDPNCs to variation of environmental pH value is a desirable feature for their biomedical applications. The response of CDPNCs to different pH values was investigated by monitoring the change in turbidity of the dispersion when the step-wise addition of 0.1 M NaOH was carried out. It should be noted that the pH after the formation of CDPNCs is about 3.7. As shown in **Figure 4**a, when the pH in system varies from 3.7 to 8.5, the turbidity slightly declines. It can be explained that partly aggregation of CDPNCs occurs through the salt effect,[23] which can be confirmed by the relevant TEM results (Figure S7, Supporting Information). All of the results reveal the CDPNCs can exist with good stability at physiological pH condition. The stability was further assessed in cell culture medium. Figure 4b exhibits the CDPNCs are stable more than 10 days when they are added to the Dulbecco's modified Eagle's medium (DMEM) with bovine serum albumin (BSA). In this case, an increase of about 20 nm in size of CDPNCs is observed at the beginning due to protein adsorption via electrostatic attraction, which can be confirmed by the change of surface charge of CDPNCs from +28 to –12 mV. Then, the size keeps changeless with the time further extending, indicating that the CDPNCs cannot be broken by the components

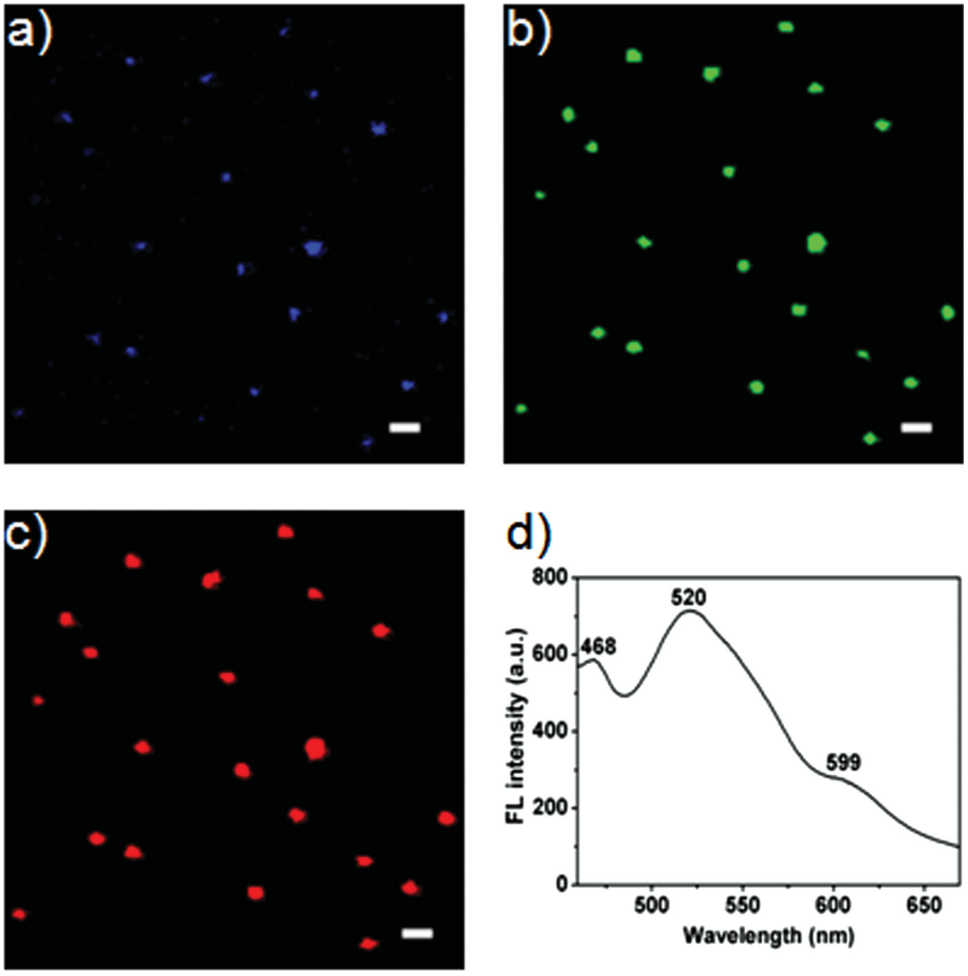

Figure 3. CLSM images of CDPNCs excited at 405 nm and collected at a) blue (430–480 nm), b) green (500–550 nm), and c) red (590–640 nm) channels. Scale bars are 1 μm. d) FL spectrum of CDPNCs powder dispersed in water excited at 405 nm.

of the biological medium and can stably exist in the biological medium.

Furthermore, the biodegradation of nanocarriers is very important for application in releasing their encapsulated cargo in the bio-system. The degradation of CDPNCs as-prepared was demonstrated in vitro. Tyrisin was chosen as a representative of enzymes. The CDPNCs were co-incubated with tyrisin in PBS (pH = 7.2) at 37 °C. CLSM and TEM were employed to monitor the detailed degradation process of CDPNCs at different times. As shown in Figure S8 (Supporting Information), when the incubation time is 1 day, in comparison with incubation in PBS without tyrisin, the sharp reduction of red dots originating from fluorescence of CDPNCs is clearly observed. As incubation time is prolonged to 10 days, CDPNCs in PBS without tyrisin only slight decrease, while CDPNCs with tyrisin are left very few and are seldom observed. To further verify the degradation of CDPNCs, TEM was used to monitor the morphology variation of CDPNCs incubated with tyrisin. Compared with original morphology of CDPNCs (**Figure 5**a), most CDPNCs with different size holes are clearly visible after incubated for 1 day (Figure 5b). With the incubation time extending, the holes in CDPNCs become gradually larger and larger (Figure 5c). When incubation time is prolonged to 10 days, it is very hard to find intact spherical structure and only slight edge of CDPNCs rather than CDPNCs with holes are observed (Figure 5d). These results exhibit that CDPNCs can be degraded by tyrisin at physiological pH condition, indicating it is possible CDPNCs are degradable in the cells under the action of enzymes.

CLSM imaging 3D reconstruction was used to investigate intracellular distribution of CDPNCs after cells were incubated with CDPNCs for 1 day. As revealed in **Figure 6**, the right and bottom images showed that a few CDPNCs appeared in the cytoplasm, indicating they were enveloped by the cells membrane through endocytosis.[24] Furthermore, to confirm biodegradation of CDPNCs at the cellular level, they were co-incubated with HeLa cells in the biological medium DMEM with BSA for 10 days at 37 °C in 5% CO_2. As shown in **Figure 7**a, after incubation for 2 days, most CDPNCs were enveloped. As the incubation time was extended to 4 days, it was noted that reduction of CDPNCs was clearly displayed (Figure 7b). When the incubation time was further extended to 7 days, CDPNCs became less and less in the cells (Figure 7c). So, a fascinating result was gained that CDPNCs could be biodegraded in the cells. Finally, to further verifying the result, we prolonged incubation time

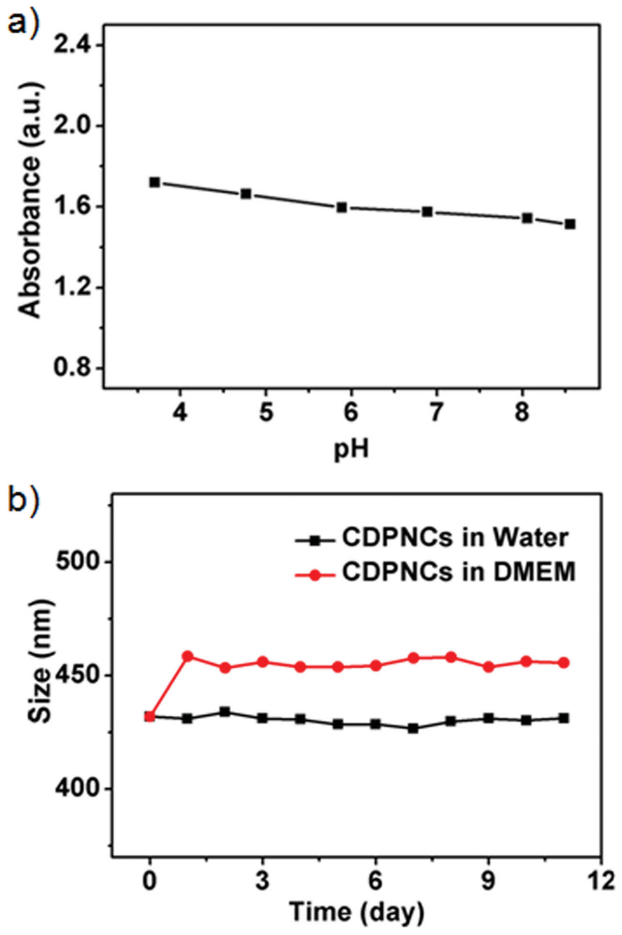

Figure 4. a) Turbidity of CDPNCs at different pH values. b) Size changes of CDPNCs over time in the DMEM with BSA after dispersing CDPNCs to DMEM.

to 10 days and found that CDPNCs were very few and almost disappeared (Figure 7d), suggesting that CDPNCs were indeed degraded in the cells. The enzymes in the cells played a crucial role in the biodegradation of the CDPNCs.

2.3. Encapsulation and Enzyme-Responsive Release of Drug Molecule

The incorporation of multi-functional molecules in the self-assemble units is beneficial to improve their function. The CDPNCs exhibit an adaptive encapsulation property of small dye molecules. Water-soluble molecules including negatively charged Congo red (CR) and positively charged Methylene blue (MB) and water-insoluble Nile red (NR) were chosen as model molecules to assess their envelopment into the CDPNCs. The colored precipitates emerged at the bottom of the centrifuge tube when the bulky solution was treated by the ultracentrifugation and the supernatant kept colorless (Figure S9, Supporting Information), indicating these small dye molecules were successfully enveloped into the CDPNCs.

As mentioned above, the CDPNCs could be loaded with small functional molecules and disassembled by enzymes at physiological pH values and in cells, which is expected that this property could be exploited for smart drug delivery.[25] In our case, DOX, one of chemotherapeutic agents for cancer treatment,[3b,26] was selected as model drug. The DOX was loaded into CDPNCs by adding 1 mL of GA/DOX solution into 8 μL of CDP/HFP solution with 1 mg of CDP. Aging for 24 h, the colored precipitates and the colorless supernatant (**Figure 8**a) indicated the DOX molecules were successfully enveloped into the CDPNCs to form CDPNCs-DOX complex. It was further confirmed by relevant ultraviolet-visible (UV–Vis) spectra. The absorption peak at 485 nm in CDPNCs-DOX spectrum was evidently raised by comparison with that of pure CDPNCs with the same concentration (Figure 8b). As shown in Figure 8c, the amount of DOX encapsulation has a reliance on DOX concentration and the loading efficiency arrives to more than 50% with an improvement of the DOX concentration. Moreover, the size of CDPNCs after loading with DOX is easily tuned through varying the concentration of DOX. As shown in Figure S10 (Supporting Information), the size of CDPNCs-DOX gradually declines when the concentration of DOX is increased. The reason may be ascribed to the electrostatic repulsion interaction between CDP and DOX. Importantly, the kinetic DOX release profiles of CDPNCs-DOX were achieved at 37 °C in PBS (pH 7.2) with and without tyrisin through monitoring the UV–Vis intensity of released DOX over time. As shown in Figure 8d, one can see that the rate of DOX released from CDPNCs-DOX in PBS without tyrisin is very slow and the quantity of release is only about 12.7 ± 0.3% within 10 days (black curve). In contrast, the profile obtained for the CDPNCs-DOX incubated with tyrisin in PBS displays a faster DOX release at the same time, and the amount of release is increased to 75.3 ± 1.4%. A plausible reason for the remarkably increase of DOX release could be attributed to the enzyme-induced degradation of CDPNCs-DOX at physiological pH condition.

2.4. Drug Delivery in Cells In Vitro

CLSM was also employed to visually investigate the DOX release of CDPNCs-DOX in HeLa cells as a function of time by monitoring the strongly red fluorescence signals of excited DOX. In this case, the blue nuclei were stained by Hoechst 33342 excited by 405 nm laser and the red fluorescent area represented CDPNCs-DOX excited by 559 nm laser. When the cells were incubated without the CDPNCs-DOX (**Figure 9**a), there were very little red fluorescence in the cells. After incubation with CDPNCs-DOX for 24 h, one can see many CDPNCs-DOX entered the cells and adhered to the nuclei. At this moment, the majority of cells were alive (Figure 9b). More importantly, the bright red fluorescence at both the cytoplasm and the nuclei verified DOX released from the CDPNCs-DOX after the cellular uptake. As shown in Figure 9c, after a further culturing for 24 h, the red fluorescence was continually increased at a DOX-rich site including the cytoplasm and the nuclei and overlapped the blue fluorescence of nuclei to exhibit the pink fluorescence of nuclei. Meanwhile, only a minority of surviving cells were left. Based on the results above, it could be proposed that after the CDPNCs-DOX are encapsulated through the endocytosis by cells, the release of DOX is induced

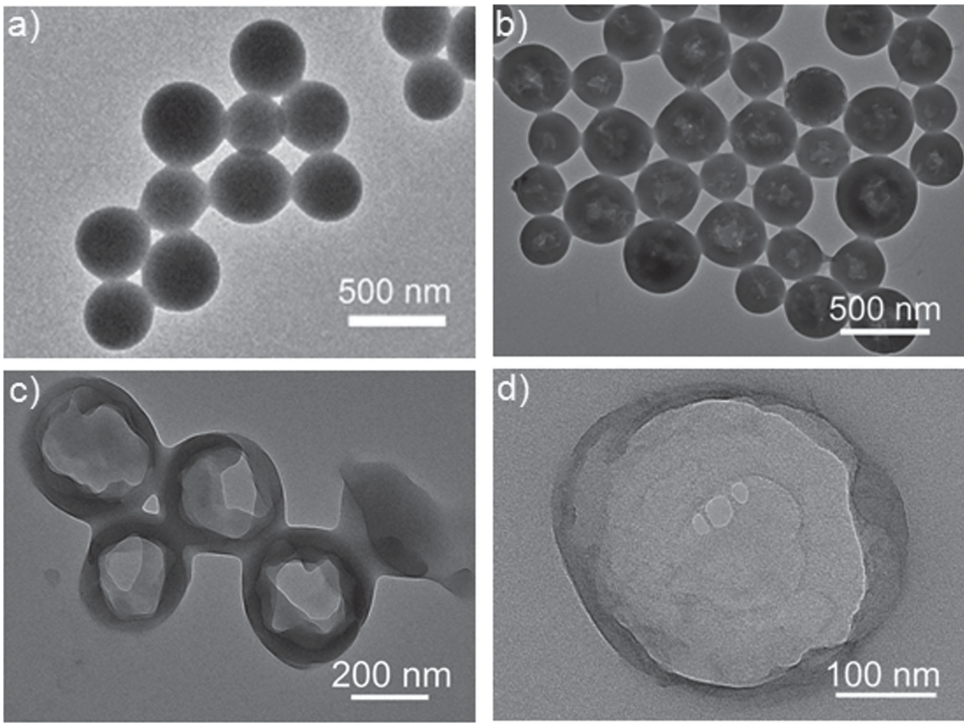

Figure 5. TEM images of CDPNCs co-incubated with tyrisin in PBS (pH 7.2) at 37 °C for different times. a) 0, b) 1, c) 5, and d) 10 days.

by the action of enzymes and then the released DOX have an accumulation in the cell nuclei, and finally result in the cancer cells death.

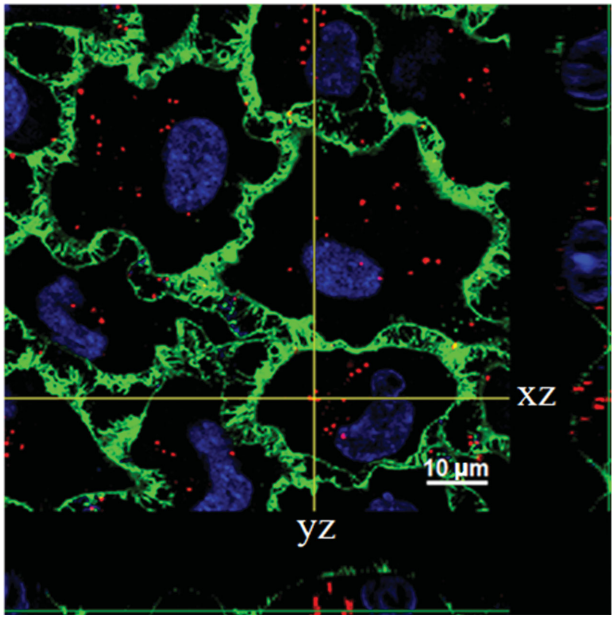

Figure 6. A 3D CLSM image of HeLa cells was scanned along *z* to form *x*–*z* and *y*–*z* sections. The two yellow lines represent *x*–*z* (bottom) and *y*–*z* (right) side views at a given z. Blue nuclei excited by 405 nm laser and green membrane excited by 488 nm laser were stained by Hoechst 33342 and Alexa 488, respectively. Red dots are the CDPNCs with autofluorescence excited by 559 nm laser.

2.5. Biocompatibility of CDPNCs and Highly Cytotoxicity Even at a Low Drug Concentration of Drug-Loaded CDPNCs

In order to evaluate the biocompatibility of CDPNCs and cytotoxicity of CDPNCs-DOX, the 3-(4,5-dimethylthiazolyl-2)-2,5-diphenyltetrazolium bromide (MTT) assay were carried out after their incubation with HeLa or COS-7 cells for different times. As shown in **Figure 10**a,b, almost 100% of both HeLa and the COS-7 cells were alive when the co-cultured concentration of CDPNCs was about 50 μg/mL. When the concentration of CDPNCs was increased and the incubation time was prolonged, the cell viability stayed more than 90%. These results show that the CDPNCs are high biocompatibility and could be used as a potential material for biomedical application in future. As a comparison, when CDPNCs-DOX with different concentration was incubated with HeLa cells, the nanocomplexes showed obvious cytotoxicity. In detail, the cancer cells and CDPNCs-DOX were cultured for 48 h at equivalent DOX doses of 0.2, 0.4, 0.6 and 0.8 μg/ml, respectively. As shown in Figure 10c, the cell viability was notably reduced from 35% to 20% when raising the DOX concentration from 0.2 to 0.8 μg/mL, indicating the concentration-dependent cytotoxicity of CDPNCs-DOX. Meanwhile, the impact of incubation time on cell viability was investigated when DOX dose was fixed at 0.8μg/ml. Figure 10d displayed a time-dependent cytotoxicity of CDPNCs-DOX and the cell viability obviously decreased from 81% (24 h) to 45% (36 h) and further to 20% (48 h). This result also confirms that the DOX release from the CDPNCs-DOX after cellular internalization is a long-term process. Importantly, in contrast, the cells cultured with

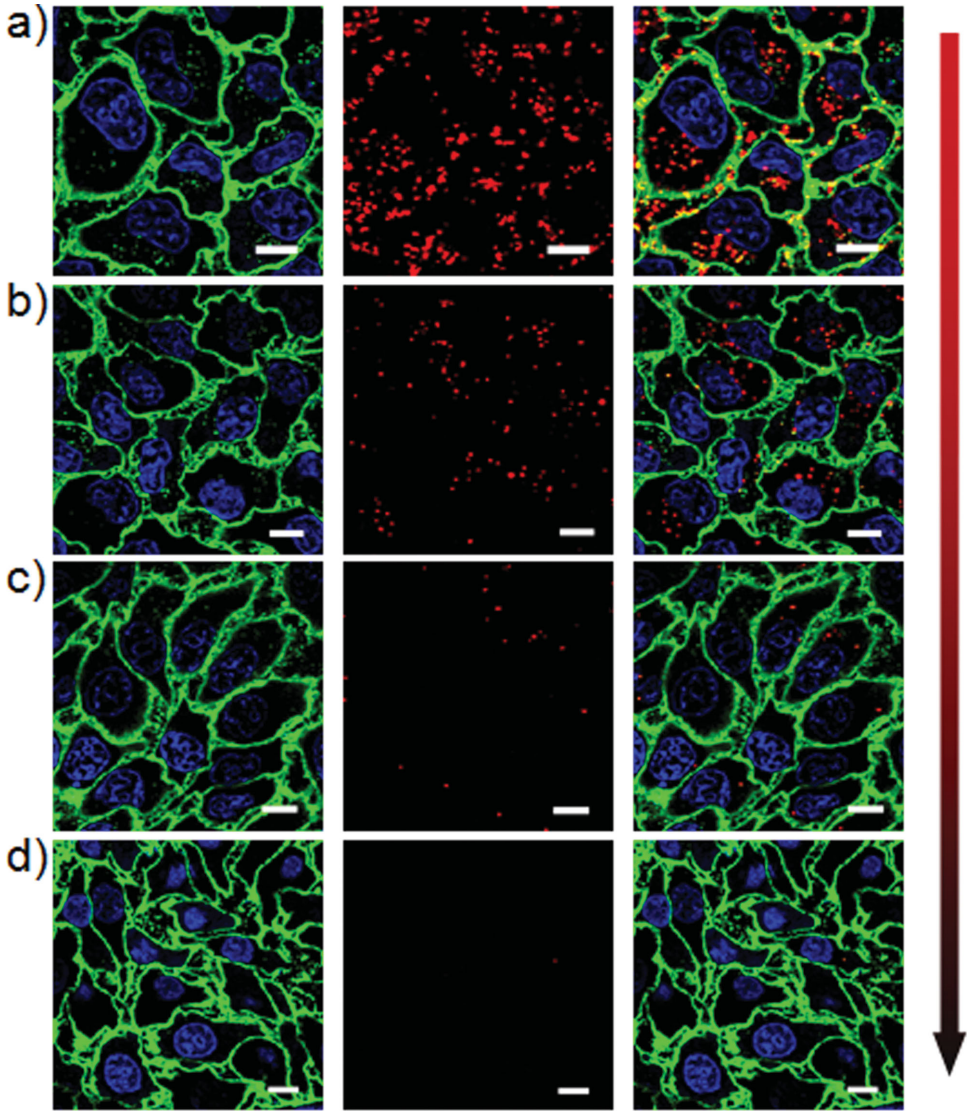

Figure 7. CLSM images of CDPNCs degraded in HeLa cells over time. Blue nuclei excited by 405 nm laser and green membrane excited by 488 nm laser were stained by Hoechst 33342 and Alexa488, respectively. Red dots are CDPNCs excited by 559 nm laser. CDPNSs and HeLa cells were co-incubated for different times. a) 2, b) 4, c) 7, and d) 10 days. Scale bars are 10 μm. The intensity of 559 nm laser was fixed and kept constant in all experiments.

the equivalent dose of free DOX have a lower mortality rate than incubated with CDPNCs-DOX at the same incubation time. The possible reasons could be deduced as follows. On one hand, HeLa cells have a powerful resistance to free DOX at the very low concentration.[2b] On the other hand, the CDPNCs could protect DOX from consumption in the process of cell metabolism and extend the retention time of drug in the cells and then enhance cytotoxicity of DOX. Taken together, the CDPNCs possess excellent biocompatibility for both cancer and normal cells. After uploading DOX, even at a very low concentration of drug, the nanocomplexes exhibit a high cytotoxicity against tumor cell proliferation. It also means the amount of anticancer drug can be decreased to kill the same quantity of cancer cells, which is desirable for cancer therapy in vivo in future.

3. Conclusions

In summary, we successfully obtained the monodisperse dipeptide-based nanocarriers with tunable size in a controlled manner through small-molecule-induced covalent assembly. They have shown the obvious autofluorescence, high biocompatibility and excellent biodegradation. Such assembled structure is rather stable in water as well as in PBS (pH 7.2). Meanwhile, they can also be readily disassembled by tyrisin in PBS. Furthermore, the nanocarriers can be utilized to encapsulate and transport chemotherapeutic agents like DOX and the loading capacity can reach over 50%. With the in vitro experiments, we found that the release kinetics of DOX in PBS (pH 7.2) is a remarkably faster with the existence of tyrisin, comparing to that without tyrisin, indicating the enzyme-responsive

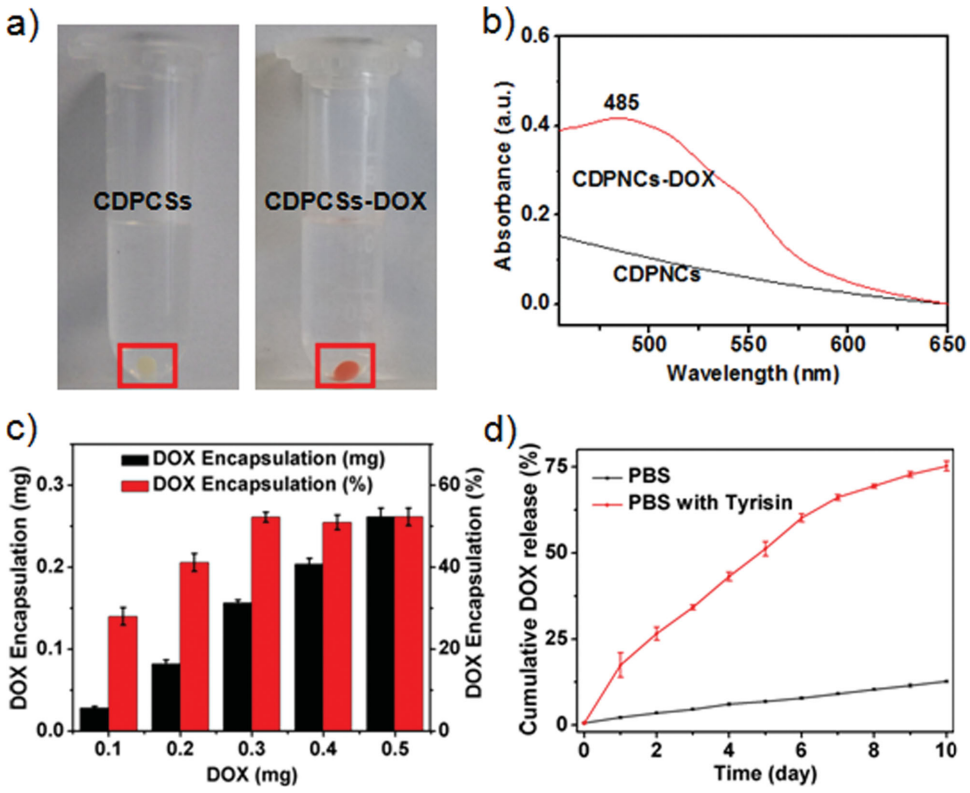

Figure 8. a) The photo images of CDPNCs and CDPNCs-DOX in pure water before (left) and after (right) loading with DOX. b) UV–Vis spectra of CDPNCs at the same concentration before (black curve) and after (red curve) loading with DOX. c) The encapsulated quantity of DOX by 1 mg of CDP under the different initial total amount of DOX in the 1 mL of solution. d) Cumulative quantitive analysis of DOX released from CDPNCs-DOX in pH 7.2 PBS with and without tyrisin by UV–Vis spectra.

property. Correspondingly, the assembled CDPNCs-DOX has much higher efficiency against tumor cell proliferation even at a very low concentration, compared with free DOX. We thus developed a new type of enzyme-responsive nanocarriers for the biomedical application in the treatment of cancer.

4. Experimental Section

Materials: Cationic dipeptide (H-Phe-Phe-NH_2·HCl, CDP) was purchased from Bachem (Bubendorf, Switzerland). Glutaraldehyde (GA), 1,1,1,3,3,3-hexafluoro-2-propanol (HFP), Hoechst 33342 and Nile red (NR) were purchased from Sigma-Aldrich. Phenylalanine (F), Congo red (CR), methylene blue (MB), sodium hydroxide (NaOH) and dimethyl sulfoxide (DMSO) were bought from Beijing Chemical Reagent Ltd, China. 3-(4,5-Dimethylthiazolyl-2)-2,5-dipheny tetrazolium bromide (MTT) was obtained from Amresco. Alexa Fluor 488 was bought from Molecular Probes Inc. Medium Dulbecco's Modified Eagle medium (DMEM) and bovine serum albumin (BSA) were purchased from Invitrogen. Doxorubicin (DOX) was bought from Aladdin. All the materials were commercially available and used directly without further purification unless otherwise mentioned. The ultrapure water used in all experiments was prepared in a Milli-Q Plus 185 purification system (Millipore) with a resistivity of 18.2 MΩ cm.

Preparation of Cationic Dipeptide Nanocarriers (CDPNCs): The preparation of CDPNCs was typically performed as follows: 1 mg cationic dipeptide (CDP) was dissolved in 8 μL of 1,1,1,3,3,3-hexafluoro-2-propanol (HFP). Afterwards, 1 mL of 0.06% glutaraldehyde (GA) solutions was added. Aging for 24 h later, yellowish precipitates yielded. To eliminate the cytotoxic HFP and residual GA, the precipitates were centrifuged, washed three times using ultra-pure water and kept in Milli-Q water at room temperature for using in the following experiments.

Preparation of Phenylalanine Nanoparticles (FNPs): The preparation of FNPs was typically performed as follows: 20 mg F was dissolved in 1 mL of ultra-pure water. Afterwards, 24 μL of 25% GA solutions was added. Aging for 12 h, yellow precipitates yielded. To eliminate residual GA, the precipitates were centrifuged, washed three times and kept in Milli-Q water at room temperature for the following experiments.

Microscopy: scanning electron microscopy (SEM) images were obtained by an S-4800 (HITACHI, Japan) with 10 kV accelerating voltage. For SEM sample, 5 μL of CDPNCs or CDPNCs-DOX suspension was placed onto silicon substrates and dried in vacuum. Transmission electron microscopy (TEM) were performed by a JEOL JEM-1011 (100 kV) when a drop of sample was carefully picked up and applied to the carbon-coated copper grids and dried in vacuum. Cryo-TEM images were gained by a Tecnai Spirit 120 kV (100 kV) when the sample was placed onto the copper grids and freezed under liquid nitrogen condition. CLSM images were obtained by Olympus FV500 with 60× oil-immersion objectives and a numerical aperture of 1.4.

Spectroscopy: Fourier transform infrared spectroscopy (FTIR) spectra were required on a Bruker EQUINOX 55/S Spectrophotometer through carefully placing samples onto CaF_2 pellets. X-ray photoelectron spectroscopy (XPS) spectra were performed by a VG ESCA-LAB 220i-XL. A Bruker BIFLEX III mass spectrometer was employed to collect the matrix-assisted laser desorption/ionization time-of-flight mass spectrometry (MALDI-TOF-MS) in reflector mode (α-cyano-4-hydroxycinnamic acid was used as matrix for ionization of the sample). Thermogravimertric analysis (TGA) of CDPNCs was measured by a Pyris Diamond TG-DTA (Perkin-Elmer instrument). The samples were heated

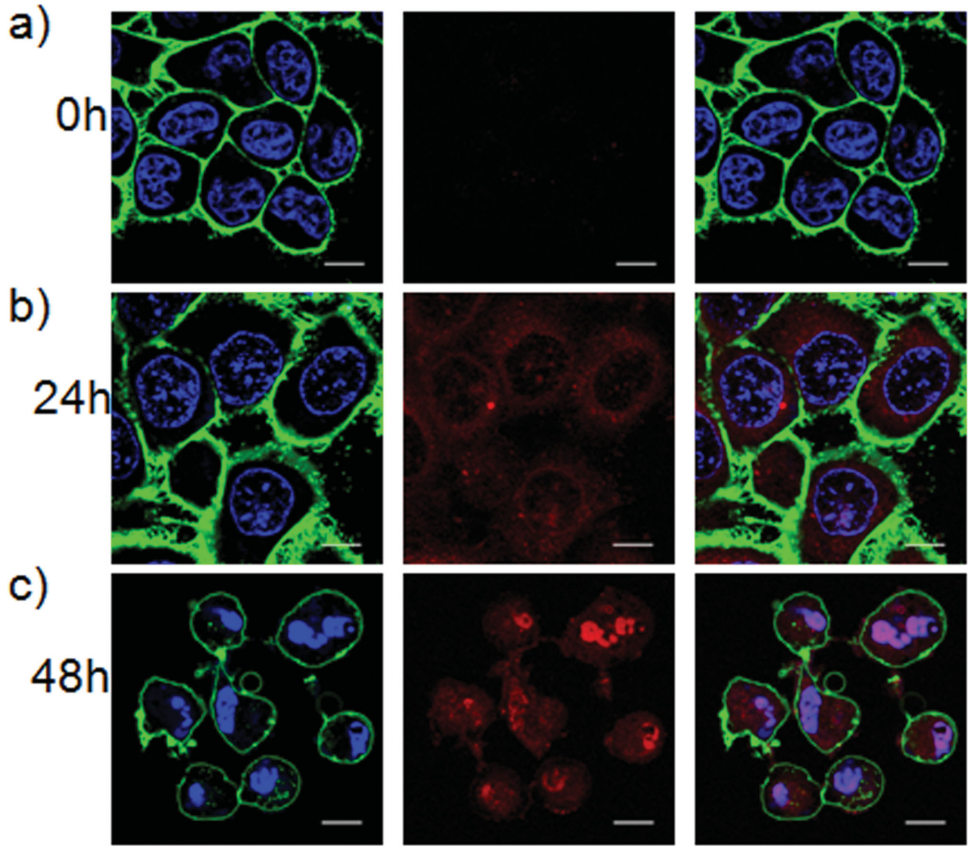

Figure 9. CLSM images of drug release behavior of CDPNCs-DOX after cellular uptake at different time. Blue nuclei excited by 405 nm laser and green membrane excited by 488 nm laser were stained by Hoechst 33342 and Alexa 488, respectively. Red fluorescenceis CDPNCs-DOX excited by 559 nm laser. CDPNCs and HeLa cells were co-incubated for different times. a) 0, b) 24, and c) 48 h. Scale bars are 10 μm. The intensity of 559 nm laser was fixed and kept constant in all experiments.

from 45 to 500 °C at a constant rate of 5 °C min under a N_2 atmosphere. Before the TGA, the samples were dried under vacuum until constant weight. Fluorescence emission spectrum (FL) of CDPNCs in water was recorded by A Hitachi Model F-4500 spectrofluorimeter. Ultraviolet-visible spectra (UV–Vis) of all samples were recorded by a Hitachi U-3100 spectrophotometer.

Stability of CDPNCs Under Different Condition: The stability of CDPNCs to variation of environmental pH value was investigated by UV–Vis spectra and TEM measurements. When 0.1 M NaOH was added into CDPNCs suspension by a step-wise fashion, the change in turbidity of the dispersion at a wavelength of 650 nm was recorded by UV–Vis spectra and the structures of CDPNCs at different pH were observed by TEM images. The stability was further assessed in cell culture medium by DLS measurements. After centrifuged, CDPNCs was kept in DMEM with the same volume for more than ten days and the hydrodynamic size of CDPNCs was monitored by DLS every day.

Drug Loaded by Cationic Dipeptide Nanocarriers and Enzyme-responsive ReleaseIn Vitro: The incorporation of DOX into the CDPNCs through a co-precipitation method was typically carried out in detail described below: 1 mg cationic dipeptide (CDP) was dissolved in 8 μL of 1,1,1,3,3,3-hexafluoro-2-propanol (HFP). Afterwards, 1 mL of 0.06% glutaraldehyde (GA) solutions with the different amount of DOX (0.1, 0.2, 0.3, 0.4, and 0.5 mg) was added. Aging for 24 h later, red precipitates (CDPNCs-DOX) yielded. To eliminate the cytotoxic HFP and residual GA and unloaded DOX, the precipitates were centrifuged, washed using ultra-pure water until the supernatant was colorless and then kept in Milli-Q water at room temperature for using in the following experiments. The amount of DOX loaded into CDPNCs was determined by UV–Vis spectra and the loading efficiency (LE%) was calculated through the following equation:

$$\mathrm{LE\%} = \left(\frac{\text{amount of DOX in CDPNCs}}{\text{total amount of DOX in the initial solution}}\right) \times 100\% \quad (1)$$

In vitro, the enzyme-responsive release of DOX from DOX-loaded CDPNCs was carried out in PBS (pH 7.2) with tyrisin and the release in PBS (pH 7.2) without tyrisin was used as the comparison. Firstly, the standard curve of DOX in PBS (pH 7.2) was generated according to the absorbance of DOX at 485 nm when the concentration of DOX was varied from 0.1 to 30 μg/mL (Figure S11, Supporting Information). Then, after centrifuged, the DOX-loaded CDPNCs were suspended into the 3 mL of tyrisin solution (2 mg/mL) and then the suspension was placed into the water bath with 37 °C. The release medium was taken out after centrifuged and was substituted for the fresh release medium with equivalent volume every 24 h. The release amount of DOX was assayed by UV–Vis spectroscopy based on the standard curve (Figure S11, Supporting Information) and the release experiments were performed in triplicate.

Cell Culture and Intracellular Biodegradation of CDPNCs: HeLa cells was employed for intracellular location and biodegradation of CDPNCs and the cells were cultured in DMEM medium with BSA (10%), penicillin (1%) and streptomycin at 37 °C in 5% CO_2 and 70% humidity. As the cells grew to 80% confluence and then were washed by pH 7.2 PBS, trypsinized and reseeded into several 35 mm Petri dishes with fresh DMEM. After 24 h, to observe the biodegradation, 20 μL of CDPNCs (6 mg/mL) suspension was added to the Petri dishes and co-cultured with the cells for different time 2, 4, 7, and 10 days, respectively. After co-cultivation for 2 days, the residual CDPNCs were removed. Since that time, cell culture medium was substituted for fresh DMEM every day until imaged.

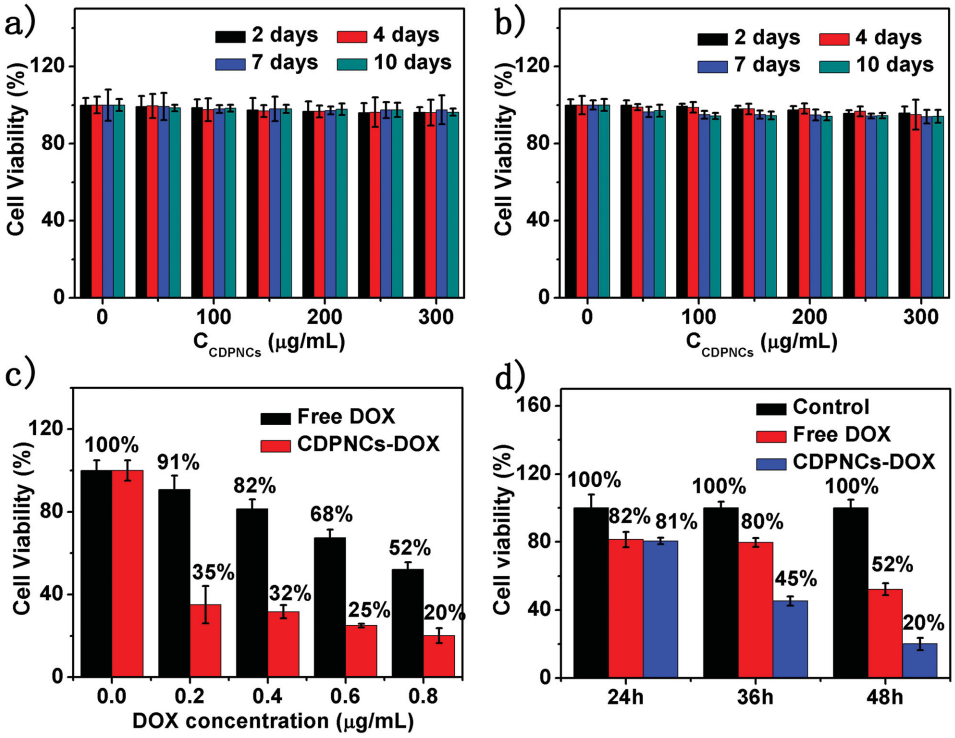

Figure 10. a,b) Cytotoxicity studies of CDPNCs for different cells, different incubation times as a function of the concentration of CDPNCs. a) HeLa cells and b) COS-7 cells. c) Cytotoxicity of CDPNCs-DOX for HeLa cells incubated for 48 h with different DOX concentration. d) Cytotoxicity of CDPNCs-DOX with a fixed DOX concentration (0.8 μg/mL) for HeLa cells incubated for different time.

Cytotoxicity Assay: The HeLa cells and COS-7 cells as canner cell and normal cell representative respectively, were used for the cytotoxicity research of CDPNCs. The cells were split into 96-well or 48-well plates through a standard tyrisin-based technique. After 24 h, CDPNCs was added to the per-well to co-culture with the cells and the concentration of CDPNCs was 0, 50, 100, 150, 200, 250, and 300 μg/mL in the different wells on the same plate, respectively. Co-incubation for different times 2, 4, 7, and 10 days, MTT (20 μL, 5 mg/mL) in PBS was added to every well and incubated with cells for 4 h at 37 °C in 5% CO_2. Then, the culture medium with MTT was replaced by DMSO to dissolve the purple formazan crystals produced through interaction between the living cells and MTT. The absorbance at a wavelength of 490 nm was measured by a wallac 1420 multilabel counter. Next, The HeLa cells were selected for the cytotoxicity study of CDPNCs-DOX. When the cells were split into 96-well and cultured for 24 h, free DOX and CDPNCs-DOX with the same concentration of DOX were added into the different well on the same plate. Then, the cytotoxicity results were obtained through the above method after 24, 36, and 48 h.

Supporting Information

Supporting Information is available from the Wiley Online Library or from the author.

Acknowledgements

The authors acknowledge the financial support of this work by the National Nature Science Foundation of China (No. 21320102004, 21433010, 91027045, 21273250, 51303038), the National Basic Research program of China (973 program, 2013CB932802) and Institute of Chemistry, Chinese Academy of Science (CMS-PY-201322).

Received: September 9, 2014
Revised: October 29, 2014
Published online: November, 20, 2014

[1] V. R. Devadasu, V. Bhardwaj, M. N. V. R. Kumar, *Chem. Rev.* **2013**, *113*, 1686–1735.
[2] a) S. Mura, J. Nicolas, P. Couvreur, *Nat. Mater.* **2013**, *12*, 991–1003; b) Q. Yin, J. N. Shen, Z. W. Zhang, H. J. Yu, Y. P. Li, *Adv. Drug Delivery Rev.* **2013**, *65*, 1699–1715; c) C. Alvarez-Lorenzo, A. Concheiro, *Chem. Commun.* **2014**, *50*, 7743–7765.
[3] a) J. Liu, Y. R. Huang, A. Kumar, A. Tan, S. B. Jin, A. B. Mozhi, X. J. Liang, *Biotechnol. Adv.* **2014**, *32*, 693–710; b) P. Moitra, K. Kumar, P. Kondaiah, S. Bhattacharya, *Angew. Chem. Int. Ed.* **2014**, *53*, 1113–1117; *Angew. Chem.* **2014**, *126*, 1131–1135; c) F. F. Zhao, G. Z. Shen, C. J. Chen, R. R. Xing, Q. L. Zou, G. H. Ma, X. H. Yan, *Chem. Eur. J.* **2014**, *20*, 6880–6887.
[4] a) A. J. Harnoy, I. Rosenbaum, E. Tirosh, Y. Ebenstein, R. Shaharabani, R. Beck, R. J. Amir, *J. Am. Chem. Soc.* **2014**, *136*, 7531–7534; b) M. Zelzer, S. J. Todd, A. R. Hirst, T. O. Mcdonald, R. V. Ulijn, *Biomater. Sci.* **2013**, *1*, 11–39.
[5] a) C. L. Shi, X. Guo, Q. Q. Qu, Z. M. Tang, Y. Wang, S. B. Zhou, *Biomaterials* **2014**, *35*, 8711–8722; b) Y. Y. Zhuang, Y. Su, Y. Peng, D. L. Wang, H. P. Deng, X. D. Xi, X. Y. Zhu, Y. F. Lu, *Biomacromolecules* **2014**, *15*, 1408–1418; c) M. Huo, J. Y. Yuan, L. Tao, Y. Wei, *Polym. Chem.* **2014**, *5*, 1519–1528.
[6] a) Z. C. Zhu, N. Gao, H. J. Wang, S. A. Sukhishvili, *J. Controlled Release* **2013**, *171*, 73–80; b) Z. S. Al-Ahmady, W. T. Al-Jamal,

J. V. Bossche, T. T. Bui, A. F. Drake, A. J. Mason, K. Kostarelos, *ACS Nano* **2012**, *10*, 9335–9346.
[7] a) J. F. Gohy, Y. Zhao, *Chem. Soc. Rev.* **2013**, *42*, 7117–7129; b) J. Gao, S. S. Huang, Y. Q. Chen, S. W. Li, X. Li, D. W. Deng, Z. Y. Qian, L. P. Tang, Y. Q. Gu, *Biomaterials* **2013**, *34*, 6272–6283.
[8] J. Thévenot, H. Oliveira, O. Sandre, S. Lecommandoux, *Chem. Soc. Rev.* **2013**, *42*, 7099–7116.
[9] a) W. C. Chen, Y. Y. Yuan, D. Cheng, J. F. Chen, L. Wang, X. T. Shuai, *Small* **2014**, *10*, 2678–2687; b) Y. C. Chen, L. C. Liao, P. L. Lu, C. L. Lo, H. C. Tsai, C. Y. Huang, K. C. Wei, T. C. Yen, G. H. Hsiue, *Biomaterials* **2012**, *33*, 4576–4588.
[10] a) Q. L. Zhou, L. Zhang, X. H. Yan, A. H. Wang, G. H. Ma, J. B. Li, H. Möhwald, S. Mann, *Angew. Chem. Int. Ed.* **2014**, *53*, 2366–2370; *Angew. Chem.* **2014**, *126*, 2398–2402; b) Z. F. Sun, Z. Y. Li, Y. H. He, R. J. Shen, L. Deng, M. H. Yang, Y. Z. Liang, Y. Zhang, *J. Am. Chem. Soc.* **2013**, *135*, 13379–13386; c) Y. Ikezoe, G. Washino, T. Uemura, S. kitagawa, H. Matsui, *Nat Mater* **2012**, *11*, 1081–1085; d) J. H. Kim, M. Lee, J. S. Lee, C. B. Park, *Angew. Chem. Int. Ed.* **2012**, *51*, 517–520; *Angew. Chem.* **2012**, *124*, 532–535; e) X. H. Yan, Y. Su, J. B. Li, J. Früh, H. Möhwald, *Angew. Chem. Int. Ed.* **2011**, *50*, 11186–11191; *Angew. Chem.* **2011**, *123*, 11382–11387; f) X. H. Yan, J. B. Li, H. Möhwald, *Adv. Mater.* **2011**, *23*, 2796–2081; g) X. H. Yan, P. L. Zhu, J. B. Li, *Chem. Soc. Rev.* **2010**, *39*, 1877–1890; h) L. Adler-Abramovich, D. Aronov, P. Beker, M. Yevnin, S. Stempler, L. Buzhansky, G. Rosenman, E. Gazit, *Nat. Nanotechnol.* **2009**, *4*, 849–854.
[11] M. Reches, E. Gazit, *Science* **2003**, *300*, 625–627.
[12] a) J. Y. Li, Y. Kuang, Y. Gao, X. W. Du, J. F. Shi, B. Xu, *J. Am. Chem. Soc.* **2013**, *135*, 542–545; b) W. T. Zheng, J. Gao, L. J. Song, C. Y. Chen, D. Guan, Z. H. Wang, Z. B. Li, D. L. Kong, Z. M. Yang, *J. Am. Chem. Soc.* **2013**, *135*, 266–271; c) C. W. Ou, J. W. Zhang, X. L. Zhang, Z. M. Yang, M. S. Chen, *Chem. Commun.* **2013**, *49*, 1853–1855; d) Y. Y. Ding, D. Li, K. Zhao, W. Du, J. Y. Zheng, M. H. Yang, *Biosens. Bioelectron.* **2013**, *48*, 281–286; e) Z. P. Huang, S. W. Guan, Y. G. Wang, G. N. Shi, L. N. Cao, Y. Z. Gao, Z. Y. Dong, J. Y. Xu, Q. Luo, J. Q. Liu, *J. Mater. Chem. B.* **2013**, *1*, 2297–2304; f) L. Chen, G. Pont, K. Morris, G. Lotze, A. Squires, L. C. Serpell, D. J. Adams, *Chem. Commun.* **2011**, *47*, 12071–12073; g) Y. Kuang, Y. Gao, B. Xu, *Chem. Commun.* **2011**, *47*, 12625–12627; h) G. Charalambidis, E. Kasotakis, T. Lazarides, A. Mitraki, A. G. Coutsolelos, *Chem. Eur. J.* **2011**, *17*, 7213–7219; i) Z. M. Yang, G. L. Liang, L. Wang, B. Xu, *J. Am. Chem. Soc.* **2006**, *128*, 3038–3043.
[13] a) M. B. Taskin, L. Sasso, M. Dimaki, W. E. Svendsen, J. Castillo-León, *ACS Apple. Mater. Interfaces* **2013**, *5*, 3323–3328; b) X. H. Yan, Q. He, K. W. Wang, L. Duan, Y. Cui, J. B. Li, *Angew. Chem. Int. Ed.* **2007**, *46*, 2431–2434; *Angew. Chem.* **2007**, *119*, 2483–2486; c) X. H. Yan, Y. Cui, Q. He, K. W. Wang, J. B. Li, *Chem. Mater.* **2008**, *20*, 1522–1526; d) X. H. Yan, Y. Cui, W. Qi, Y. Su, Y. Yang, Q. He, J. B. Li, *Small* **2008**, *4*, 1687–1693.
[14] a) N. Hendler, N. Sidelman, M. Reches, E. Gazit, Y. Rosenberg, S. Richter, *Adv. Mater.* **2007**, *19*, 1485–1488; b) Y. L. Wang, M. Lingenfelder, T. Classen, G. Costantini, K. Kern, *J. Am. Chem. Soc.* **2007**, *129*, 15742–15743; c) J. Ryu, C. B. Park, *Adv. Mater.* **2008**, *20*, 3754–3758; d) J. Ryu, S. Y. Lim, C. B. Park, *Adv. Mater.* **2009**, *21*, 1577–1581; e) P. L. Zhu, X. H. Yan, Y. Su, Y. Yang, J. B. Li, *Chem. Eur. J.* **2010**, *16*, 3176–3183; f) Y. Su, X. H. Yan, A. H. Wang, J. B. Fei, Y. Cui, Q. He, J. B. Li, *J. Mater. Chem.* **2010**, *20*, 6734–6740; g) J. Kim, T. H. Han, Y. Kim, J. S. Park, J. Choi, D. G. Churchill, S. O. Kim, H. Ihee, *Adv. Mater.* **2010**, *22*, 583–587; h) J. S. Lee, I. Yoon, J. Kim, H. Ihee, B. kim, C. B. Park, *Angew. Chem. Int. Ed.* **2011**, *50*, 1164–1167; *Angew. Chem.* **2011**, *123*, 1196–1199; i) Z. X. Gan, X. L. Wu, X. B. Zhu, J. C. Shen, *Angew. Chem. Int. Ed.* **2013**, *52*, 2055–2059; *Angew. Chem.* **2013**, *125*, 2109–2113; j) P. Li, X. Chen, W. S. Yang, *Langmuir* **2013**, *29*, 8629–8635.
[15] I. Migneault, C. Dartiguenave, M. J. Bertrand, C. Waldron, *BioTechniques* **2004**, *37*, 790–802.
[16] a) K. Elfrink, J. Ollesch, J. Söhr, D. Willbold, D. Riesner, K. Gerwert, *Proc. Natl. Acad. Sci. USA* **2008**, *105*, 10815–10819; b) M. S. Lamm, K. Rajagopal, J. P. Schneider, D. J. Pochan, *J. Am. Chem. Soc.* **2005**, *127*, 16692–16700.
[17] a) C. L. Du, J. Zhao, J. B. Fei, Y. Cui, J. B. Li, *Adv. Healthcare Mater.* **2013**, *2*, 1246–1251; b) L. Gao, J. B. Fei, J. Zhao, W. Cui, Y. Cui, J. B. Li, *Chem. Eur. J.* **2012**, *18*, 3185–3192; c) E. F. S. Vieira, A. R. Cestari, C. Airoldi, W. Loh, *Biomacromolecules* **2008**, *9*, 1195–1199; d) E. F. S. Vieira, A. R. Cestari, E. B. Santos, F. S. Dias, *J. Colloid Interface Sci.* **2005**, *289*, 42–47.
[18] M. C. Du, P. L. Zhu, X. H. Yan, Y. Su, W. X. Song, J. B. Li, *Chem. Eur. J.* **2011**, *17*, 4238–4245.
[19] a) J. Ryu, C. B. Park, *Chem. Mater.* **2008**, *20*, 4284–4290; b) V. L. Sedman, L. Adler-Abramovich, S. Allen, E. Gazit, S. J. B. Tendler, *J. Am. Chem. Soc.* **2006**, *128*, 6903–6908.
[20] a) W. Wei, L. Yuan, G. Hu, L. Y. Wang, J. Wu, X. Hu, Z. G. Su, G. H. Ma, *Adv. Mater.* **2008**, *20*, 2292–2296; b) W. Wei, L. Y. Wang, L. Yuan, Q. Wei, X. D. Yang, Z. G. Su, G. H. Ma, *Adv. Funct. Mater.* **2007**, *17*, 3153–3158.
[21] K. Lee, S. Choi, C. Yang, H. C. Wu, J. Yu, *Chem. Commun.* **2013**, *49*, 3028–3030.
[22] Y. Jia, J. B. Fei, Y. Cui, Y. Yang, L. Gao, J. B. Li, *Chem. Commun.* **2011**, *47*, 1175–1177.
[23] H. Wang, M. B. Hansen, D. W. P. M. Löwik, J. C. M. van Hest, Y. B. Li, J. A. Jansen, S. C. G. Leeuwenburgh, *Adv. Mater.* **2011**, *23*, H119–H124.
[24] a) X. H. Yan, J. Blacklock, J. B. Li, H. Möhwald, *ACS Nano* **2012**, *6*, 111–117; b) J. Rejman, V. Oberle, I. S. Zuhom, D. Hoekstra, *Biochem. J.* **2004**, *377*, 159–169.
[25] A. J. Harnoy, I. Rosenbaum, E. Tirosh, Y. Ebenstein, R. Shaharabani, R. Beck, R. J. Amir, *J. Am. Chem. Soc.* **2014**, *136*, 7531–7534.
[26] a) A. K. Iyer, A. Singh, S. Ganta, M. M. Amiji, *Adv. Drug Delivery Rev.* **2013**, *65*, 1784–1802; b) P. Ma, R. J. Mumper, *Nano Today* **2013**, *8*, 313–331; d) J. Li, Y. Wang, Y. Zhu, D. Oupický, *J. Controlled Release* **2013**, *172*, 589–600.